

Unusually large polarizabilities and “new” atomic states in Ba

Chih-Hao Li* and S. M. Rochester†

*Department of Physics, University of California
at Berkeley, Berkeley, California 94720-7300*

M. G. Kozlov‡

Petersburg Nuclear Physics Institute, Gatchina, 188300, Russia

D. Budker§

*Department of Physics, University of California at Berkeley,
Berkeley, California 94720-7300 and
Nuclear Science Division, Lawrence Berkeley
National Laboratory, Berkeley, California 94720*

(Dated: October 30, 2018)

Abstract

Electric polarizabilities of four low-J even-parity states and three low-J odd-parity states of atomic barium ranging from 35,600 to 36,000 cm^{-1} are investigated. The states of interest are excited (in an atomic beam) via an intermediate odd-parity state with a sequence of two laser pulses. The odd-parity states can be excited due to the Stark-induced mixing with even-parity states. The polarizabilities are measured via direct spectroscopy on the second-stage transition. Several states have tensor and scalar polarizabilities that exceed the values that might be expected from the known energy levels of barium by more than two orders of magnitude. Two of the Stark-induced transitions cannot be identified from the known energy spectrum of barium. The observations suggest the existence of as yet unidentified odd-parity energy states, whose energies and angular momenta are determined in the present experiment. A tentative identification of these states as $[\text{Xe}]6s8p\ ^3\text{P}_{0,2}$ is suggested.

PACS numbers: 32.60.+i, 32.10.-f

*Electronic address: chihhao@socrates.berkeley.edu

†Electronic address: simonkeys@yahoo.com

[‡]Electronic address: mgk@MF1309.spb.edu

[§]Electronic address: budker@socrates.berkeley.edu

I. INTRODUCTION

Polarizabilities describe how the energy levels of a system, such as an atom, shift in an external electric field. They provide a way to probe the atomic wave function at large distances from the nucleus, and are related to various physical quantities, including van der Waals constants, dielectric constants, indices of refraction, and charge-exchange cross sections. In this work, we measured the polarizabilities of seven energy levels of barium in between 35,600 and 36,000 cm^{-1} . Although polarizabilities of several levels of barium have been measured [1, 2, 3, 4, 5], those of many other states are not yet determined. Our primary motivation for this work is to obtain information that will be used in the analysis of sensitivity and possible systematic uncertainties in experiments searching for violation of Bose-Einstein statistics for photons [6].

In the first part of this work, we measured the scalar and tensor polarizabilities and, in some cases, hyperpolarizabilities of four even-parity states, $6p^2\ ^3P_2$, $6s7d\ ^3D_{1,2}$, and $5d6d\ ^3D_1$, of barium (Fig. 1). We found that three out of these four states have unusually large polarizabilities that could only be explained by the existence of as-yet-unidentified closely-lying states of odd parity.

In the second part of the work, we looked for Stark-induced transitions to the odd-parity states ranging from 35,600 to 36,000 cm^{-1} . Several Stark-induced resonances were found and classified into three sets, corresponding to transitions to electric-field-split Zeeman sublevels of three odd-parity states. One of these can be identified as the $6s8p\ ^3P_1$ state. The other two cannot be identified with the known energy levels of barium and are possibly the $6s8p\ ^3P_{0,2}$ states, which are predicted to exist, but have not been observed. We have determined their energies to be 35,648.5(1) cm^{-1} and 35,757(1) cm^{-1} respectively. The existence of these states at these energies gives a plausible explanation for the unusually large polarizabilities found in the first part of the experiment. The polarizabilities of two odd-parity states have also been determined and are reported here.

II. EXPERIMENTAL METHOD

Pulsed lasers are used to excite barium atoms in an atomic beam to the even-parity states of interest via two successive E1 transitions (Fig. 2). Fluorescence resulting from

spontaneous decay to a lower-lying state is observed with a photomultiplier tube (PMT). When an electric field is applied to the interaction region, the resonance signal is Stark-shifted and split (Fig. 3). In addition, Stark-induced transitions to neighboring odd-parity states are seen; these are also shifted and split by the electric field. The scalar and tensor polarizabilities can be derived from appropriate fitting functions relating the positions of the resolved resonance peaks and the applied electric field.

The apparatus used (Fig. 4) is largely the same as in a previous experiment [7]. The barium beam is produced with an effusion source with a multi-slit nozzle that collimates the angular spread of the beam to ≈ 0.1 rad in both the horizontal and vertical directions. The oven, heat-shielded with tantalum foil, is resistively heated to $\approx 700^\circ\text{C}$, corresponding to saturated barium pressure in the oven of ≈ 0.1 Torr and estimated atomic beam density in the interaction region, ≈ 20 cm away from the nozzle, of $\approx 10^{11}$ atoms/cm³. Residual gas pressure in the vacuum chamber is $\leq 10^{-5}$ Torr.

The electric field is supplied by two plane-parallel electrodes (angle $\leq 10^{-3}$ rad) with diameter 6.4 cm, spaced 0.9153(3) cm apart. Voltage of up to 80 kV is applied to the top electrode using a high-voltage feed-through whose design is described in detail in Ref. [7].

The laser systems in the experiment are two tunable dye lasers (Quanta Ray PDL-2) pumped by pulsed frequency-doubled Nd-YAG lasers (Quanta Ray DCR-11 and Quantel YAG580). The Quantel laser operates at a repetition rate of ≈ 10 Hz, and slaves the Quanta Ray YAG laser, so the relative timing of the two ≈ 10 -ns laser output pulses can be controlled to within ≈ 1 ns. In order to avoid shifts of the second-stage transition spectra due to the dynamic Stark effect, the relative timing of the two laser pulses is offset by ≈ 25 ns. The dyes used are Fluorescein 548 and Rhodamine 6G. For the dye laser with Fluorescein 548, the wavelength is set at 554.7 nm (on resonance with the $6s^2\ ^1S_0 \rightarrow 6s6p\ ^1P_1$ transition). The linewidth is ≈ 20 GHz and the output is linearly polarized parallel to the static electric field. The typical pulse energy is ≈ 1.5 mJ. For the dye laser with Rhodamine 6G, the wavelength is coarsely tuned from 556 nm to 570 nm by tilting the diffraction grating in the laser cavity, and finely tuned in a range of ≈ 0.2 nm near a given resonance by varying the gas (N_2) pressure in the laser-oscillator-cavity chamber. The laser line width is ≈ 20 GHz, or ≈ 6 GHz when a narrowing etalon is employed. Typical pulse energy is 3 mJ. Color glass filters are used to reduce the pulse energy to ≈ 0.4 mJ to avoid power broadening effects. Both laser beams are ≈ 3 mm in diameter.

The two laser beams are sent into the chamber in anti-parallel directions. To block scattered light from entering the chamber, two 38-cm-long collimating arms with several knife-edge diaphragms are used for the entrance and exit of the laser beams.

Fluorescence is detected at 45° to both the atomic and laser beams with a 2-in.-diameter PMT (type EMI 9750B). The gain of the PMT is $\approx 7 \times 10^5$ and the quantum efficiency at the wavelengths used is $\approx 25\%$. Interference filters with 10-nm bandwidth are used to select the decay channel of interest, and a color glass filter is used to further reduce the scattered light from the lasers.

In the first part of this experiment, we used CAMAC modules connected through a general purpose interface bus (GPIB) to a personal computer running LABVIEW software for data acquisition. The fluorescence signal, as well as laser diagnostics, including frequency markers, are recorded. In the second part, we observed the time-dependent fluorescence signals with a digital oscilloscope and determined the resonance wavelengths of the second-stage laser from the reading of the grating position.

The frequency of the first-stage laser is set on resonance with the $6s^2\ ^1S_0$ to $6s6p\ ^1P_1$ transition. We scan the frequency of the second-stage laser across the resonance of a certain probed state with total angular momentum J . When no electric field is applied, we expect to see one resonance peak (or nothing in the case of Stark-induced transitions). The shape of the peak is mostly determined by the laser spectrum averaged over many pulses and can be approximated with a Lorentzian. When the electric field is applied along the z-axis, we expect the resonance to shift and split into $J + 1$ peaks (for the present case of integer J), corresponding to sublevels with different $|M|$, which we determined by varying the polarizations of both laser beams, observing the variations of the resonant signal amplitudes and comparing them to our expectations as following.

If the first-stage laser beam is linearly polarized along the z-axis, the atoms can be excited to the $M = 0$ sublevel of the 1P_1 intermediate state. If the second-stage laser beam is polarized along the z-axis, it can further excite the atoms to the $M = 0$ sublevel of a $J = 0$ or $J = 2$ probed state. Notice that the transition to a $J = 1\ M = 0$ sublevel is forbidden because the Clebsch-Gordan coefficient is zero. If the polarization of the second-stage laser beam is along the y-axis, the atoms can be further excited to the $|M| = 1$ sublevels of a $J = 1$ or $J = 2$ probed state.

If the first-stage laser beam is linearly polarized along the y-axis, the atoms can be excited

to a coherent superposition of $M = 1$ and $M = -1$ sublevels ($(|M = 1\rangle - |M = -1\rangle)/\sqrt{2}$) of the 1P_1 intermediate state. If the second-stage laser beam is polarized along the z-axis, it can further excite the atoms to the $|M| = 1$ sublevels of a $J = 1$ or $J = 2$ probed state. If it is polarized along the y-axis, it can further excite the atoms to the $M = 0$ sublevel of a $J = 0$ probed state or the $M = 0$ and $|M| = 2$ sublevels of a $J = 2$ probed state. Notice that the transition to a $J = 1$ $M = 0$ sublevel is forbidden because the transition amplitudes from the $M = 1$ and $M = -1$ sublevels of the 1P_1 state have the same magnitude but opposite signs so that the sum of the amplitudes is zero. The relation between the polarizations of the laser beams and the excited Zeeman sublevels of a state with total angular momentum J is summarized in Table I.

III. THEORY OF POLARIZABILITY

In this section, we briefly introduce some definitions and formulae used in this work. For a detailed discussion, see Refs. [3, 8].

The Hamiltonian for an atom in a DC electric field $\vec{E} = \mathcal{E}\hat{z}$ can be written as:

$$H = H_0 - \vec{E} \cdot \vec{D} = H_0 - \mathcal{E}\mathcal{D}_z, \quad (1)$$

where H_0 is the Hamiltonian in the absence of electric field, with eigenenergies and eigenstates $E_{a_0J_0M}$ and $|a_0J_0M\rangle$, where a_0 is electronic configuration, J_0 is total electronic angular momentum, M is its z-component, $\vec{D} = -e\vec{r}$ is the electric dipole operator, and e is the magnitude of the electron charge. If there are only two states, exact eigenenergies can be obtained from the secular equation:

$$\begin{vmatrix} -\delta_S E_{a_0J_0M} & -\mathcal{E}\mathcal{D}_z \\ -\mathcal{E}\mathcal{D}_z & -\Delta E - \delta_S E_{a_0J_0M} \end{vmatrix} = 0, \quad (2)$$

where $\Delta E = E_{a_0J_0M} - E_{a_1J_1M}$ and $\mathcal{D}_z = \langle a_1J_1M | D_z | a_0J_0M \rangle$ ($M_1 = M_0 = M$ for z-directed electric field). From Eq. (2), the Stark energy shift of state $|a_0J_0M\rangle$ is,

$$\delta_S E_{a_0J_0M} = -\frac{\Delta E}{2} \pm \sqrt{\left(\frac{\Delta E}{2}\right)^2 + \mathcal{D}_z^2 \mathcal{E}^2}, \quad (3)$$

where the sign on the right-hand side of the equation should be chosen the same as the sign of ΔE . If the electric field is weak, so that $\mathcal{D}_z^2 \mathcal{E}^2 \ll \Delta E^2/4$, Eq. (3) can be expanded in

series. To the lowest order,

$$\delta_S E_{a_0 J_0 M}^{(2)} = \frac{\mathcal{D}_z^2 \mathcal{E}^2}{\Delta E} = -\frac{\alpha_{a_0 J_0 M}}{2} \mathcal{E}^2, \quad (4)$$

where α is the static polarizability. Thus in a two-level system, one can express the polarizability as:

$$\alpha_{a_0 J_0 M} = -2 \frac{\mathcal{D}_z^2}{\Delta E}. \quad (5)$$

If there is more than one state coupled to a state $|a_0 J_0 M\rangle$, to the lowest order, the energy shift is just a sum over all contributions:

$$\delta_S E_{a_0 J_0 M}^{(2)} = \sum_{a_1 J_1} \frac{\mathcal{D}_z^2 \mathcal{E}^2}{E_{a_0 J_0 M} - E_{a_1 J_1 M}}, \quad (6)$$

so that

$$\alpha_{a_0 J_0 M} = -2 \sum_{a_1 J_1} \frac{\mathcal{D}_z^2}{E_{a_0 J_0 M} - E_{a_1 J_1 M}}. \quad (7)$$

The polarizability is usually expressed in terms of its scalar and tensor parts as:

$$\alpha_{a_0 J_0 M} = \alpha_{0, a_0 J_0} + \alpha_{2, a_0 J_0} \frac{3M^2 - J_0(J_0 + 1)}{J_0(2J_0 - 1)}. \quad (8)$$

The scalar polarizability, α_0 , represents the average shift of different M sublevels; the tensor polarizability, α_2 , represents the differential shift. For states with $J \leq 1/2$, there is no Stark-induced splitting and, therefore, α_2 is zero.

Using the formalism of the reduced matrix elements,

$$\langle a_1 J_1 M_1 | D_q | a_0 J_0 M_0 \rangle = (-1)^{J_1 - M_1} \begin{pmatrix} J_1 & 1 & J_0 \\ -M_1 & q & M_0 \end{pmatrix} \langle a_1 J_1 || D || a_0 J_0 \rangle, \quad (9)$$

the scalar and tensor polarizabilities can be expressed as:

$$\alpha_{0, a_0 J_0} = \frac{-2}{3(2J_0 + 1)} \sum_{a_1 J_1} \frac{|\langle a_0 J_0 || D || a_1 J_1 \rangle|^2}{E_{a_0 J_0 M_0} - E_{a_1 J_1 M_1}}, \quad (10)$$

$$\alpha_{2, a_0 J_0} = 4 \left(\frac{5J_0(2J_0 - 1)}{6(2J_0 + 3)(2J_0 + 1)(J_0 + 1)} \right)^{1/2}. \quad (11)$$

$$\sum_{a_1 J_1} (-1)^{J_0 + J_1 + 1} \begin{Bmatrix} J_0 & 1 & J_1 \\ 1 & J_0 & 2 \end{Bmatrix} \frac{|\langle a_0 J_0 || D || a_1 J_1 \rangle|^2}{E_{a_0 J_0 M_0} - E_{a_1 J_1 M_1}}. \quad (12)$$

Using Eq.(8), $\alpha_{a_0 J_0 M}$ can also be expressed as:

$$\alpha_{a_0 J_0 M} = A_{a_0 J_0} + B_{a_0 J_0} M^2, \quad (13)$$

where $A_{a_0 J_0} = \alpha_{0,a_0 J_0} - \alpha_2(J_0 + 1)/(2J_0 - 1)$ and $B_{a_0 J_0} = 3\alpha_2/[J_0(2J_0 - 1)]$. In this expression, it is clearly seen that the difference between the Stark-induced energy shifts of $|M|$ sublevels and that of $M = 0$ sublevel is proportional to M^2 when the energy shifts are quadratically dependent on the electric field. In the data analysis, this relation provides us with a way to determine $|M|$ for each Stark-split resonance peak for states with $J \geq 2$.

When the applied electric field is higher, but still low enough so that the perturbation theory is valid, one needs to keep the next (fourth) order terms in the expansion:

$$\delta_S E_{a_0 J_0 M} = \delta_S E_{a_0 J_0 M}^{(2)} + \delta_S E_{a_0 J_0 M}^{(4)} + \dots, \quad (14)$$

where $\delta_S E_{a_0 J_0 M}^{(2)}$ is given by Eq.(6), and

$$\begin{aligned} \delta_S E_{a_0 J_0 M}^{(4)} = & \sum_{a_1 J_1 a_2 J_2 a_3 J_3} \frac{\mathcal{D}_z^{01} \mathcal{D}_z^{12} \mathcal{D}_z^{23} \mathcal{D}_z^{30} \mathcal{E}^4}{(E_{a_0 J_0 M} - E_{a_1 J_1 M})(E_{a_0 J_0 M} - E_{a_2 J_2 M})(E_{a_0 J_0 M} - E_{a_3 J_3 M})} \\ & - \sum_{a_1 J_1 a_2 J_2} \frac{|\mathcal{D}_z^{01}|^2 |\mathcal{D}_z^{02}|^2 \mathcal{E}^4}{(E_{a_0 J_0 M} - E_{a_1 J_1 M})^2 (E_{a_0 J_0 M} - E_{a_2 J_2 M})}, \end{aligned} \quad (15)$$

where $\mathcal{D}_z^{ij} = \langle a_i J_i M | D_z | a_j J_j M \rangle$. The hyperpolarizability is defined by:

$$\delta_S E_{a_0 J_0 M}^{(4)} = -\frac{\gamma_{a_0 J_0 M}}{4!} \mathcal{E}^4. \quad (16)$$

The hyperpolarizability is usually expressed in terms of the scalar and tensor hyperpolarizabilities, γ_0 and γ_2 , γ_4 as:

$$\begin{aligned} \gamma_{a_0 J_0 M} = & \gamma_{0,a_0 J_0} + \gamma_{2,a_0 J_0} \frac{3M^2 - J_0(J_0 + 1)}{J_0(2J_0 - 1)} \\ & + \gamma_{4,a_0 J_0} \frac{35M^4 + [25 - 30J_0(J_0 + 1)]M^2 + (J_0 - 1)J_0(J_0 + 1)(J_0 + 2)}{J_0(2J_0 - 1)(2J_0 - 2)(2J_0 - 3)}. \end{aligned} \quad (17)$$

For states with $J \leq 1/2$, γ_2 and γ_4 are zero. For states with $J \leq 3/2$, γ_4 is zero. The derivation of Eq. (15) and Eq. (17) can be found in Ref. [3].

When a weak external z-directed electric field is applied, to the lowest order, the perturbed state is mixed with opposite-parity states according to:

$$|“a_0 J_0 M”\rangle = |a_0 J_0 M\rangle + \sum_{a_1 J_1} \frac{\mathcal{D}_z \mathcal{E}}{E_{a_0 J_0 M} - E_{a_1 J_1 M}} |a_1 J_1 M\rangle. \quad (18)$$

For example, a small portion of a nominally odd-parity state has even parity. The mixing amplitude is proportional to the applied electric field. Therefore, a nominally odd-parity state can be excited from the ground state via two E1 transitions when the electric field is

applied. The transition probability to this state, which is proportional to the square of the mixing amplitude, is quadratically dependent on the applied electric field. In the experiment, we detect the Stark-induced signal from the decay of the even-parity component of the nominally odd-parity state to $6s8p\ ^3P_1$, which makes the emission probability also quadratically dependent on the electric field. Therefore, for weak electric fields, the amplitude of the signal scales as the fourth power of the field. On the other hand, if the electric field is so strong that the states of opposite parity are fully mixed, the signal amplitude is almost independent of the applied electric field. Thus, the dependence of the signal amplitude on the applied electric field can be used to check the validity of the perturbation approximation.

IV. RESULTS AND DISCUSSION

This section is divided into two subsections. In the first part, we discuss the Stark effect in four even-parity states ranging from 35,600 to 36,000 cm^{-1} . The polarizabilities of three of these states are too large to be explained by the known energy spectrum of barium and imply the existence of “new” states. As shown in Fig. 1, within the energy range probed in this experiment, one may expect the $J = 0$ and $J = 2$ of $6s8p\ ^3P_J$ states that have not been identified before are candidates for these new states. In the second part, we discuss the observation of the Stark-induced transitions to the odd-parity states. Two of them cannot be identified with the known energy levels of barium. They are possibly the $6s8p\ ^3P_{0,2}$ states and their energies are determined in this experiment. With the existence of these two “new” states, the unusually large polarizabilities found in the first subsection can be plausibly explained.

The measured relative energy shifts include the Stark-induced shift of the intermediate state, $6s6p\ ^1P_1$. However, the scalar and tensor polarizabilities of the $6s6p\ ^1P_1$ state are 51(3) $\text{kHz}/(\text{kV}/\text{cm})^2$ and $-5.34(5)\ \text{kHz}/(\text{kV}/\text{cm})^2$ [9], respectively, and contribute to the shift at a level $\leq 200\ \text{MHz}$, negligible compared to the observed shifts.

A. Stark effect of even-parity states

The derived scalar and tensor polarizabilities of $6p^2\ ^3P_2$, $6s7d\ ^3D_{1,2}$ and $5d6d\ ^3D_1$ states are listed in Table II. Multiple resonance peaks are observed for each of these four states

corresponding to different values of $|M|$. Moreover, the Stark shifts of two states show significant deviation from quadratic behavior as a function of the electric field, so that the scalar and tensor hyperpolarizabilities can be measured (Table III). The detailed experimental results for these four states are discussed in the following.

a. The $6p^2\ ^3P_2$ state. With an electric field applied, three resonance peaks are observed for this state (Figs. 3, 5). We locate the centers of the peaks by fitting the data with Lorentzian functions. The peaks are put into correspondence with Zeeman sublevels using Eq. (13) and their amplitude dependence on laser polarization. Although the observed level shifts are dominated by the polarizability, we are also able to resolve the hyperpolarizability of each sublevel by fitting with Eq. (14).

The closest known state that can Stark-mix with the $6p^2\ ^3P_2\ M = 0$ sublevel is $6s8p\ ^3P_1$ [10], with $\Delta E = -52.0(2)\text{ cm}^{-1}$ (Fig. 1). If we assume that this is the dominantly coupled state, from the shift of the $M = 0$ sublevel, we find for the reduced electric dipole moment: $|(6p^2\ ^3P_2\|D\|6s8p\ ^3P_1)_{\text{two-level}}| = 14.7(2)\text{ ea}_0$ (Table IV). This is far too large, considering that the electronic configurations of these two states are different by two electrons. Thus we can conclude that the coupling to other states and/or the effects of configuration mixing are not negligible.

The closest known state that can couple to the $6p^2\ ^3P_2\ |M| = 1$ sublevels is again $6s8p\ ^3P_1$. Using the two-level approximation, we find that the reduced electric dipole moment is $|(6p^2\ ^3P_2\|D\|6s8p\ ^3P_1)_{\text{two-level}}| = 14.3(2)\text{ ea}_0$, which is again too large. However, the fact that the obtained reduced electric dipole moments derived from $M = 0$ and $|M| = 1$ sublevels are nearly the same may suggest that the $6p^2\ ^3P_2$ state and the $6s8p\ ^3P_1$ state indeed have large electric dipole coupling perhaps due to admixtures of other configurations.

There is no apparent dominant close energy state that can couple to the $|M| = 2$ sublevels. This explains the fact that the shift of the $|M| = 2$ sublevels is an order of magnitude smaller than that of $|M| = 1$ and $M = 0$ sublevels.

b. The $6s7d\ ^3D_1$ state. With electric field applied, the resonance peak is split into two peaks, corresponding to the $M = 0$ and $|M| = 1$ sublevels, respectively (Figs. 6, 7). The size of the resonance peak corresponding to the $|J = 1\ M = 0\rangle$ sublevel is more than one order of magnitude smaller because in our experimental setup, the transition to this sublevel is nominally forbidden. It is still observed most likely because of the imperfections in the direction and purity of the laser polarizations.

Neither of the curves in Fig. 7 can be adequately fit with quadratic functions at high electric fields. Therefore, the next (fourth) order terms in the perturbation expansion should be included in the fitting function and both polarizabilities and hyperpolarizabilities can be determined.

If there is a dominantly coupled state for each of the $|M|$ sublevels, the Stark energy shifts can be described by the exact solution of the two-level Hamiltonian, Eq. (3). Under this two-level approximation, the energy difference and the electric dipole couplings between the $|M|$ sublevels and their dominant coupling state can be determined separately, and the polarizabilities can be obtained from Eq. (5).

The large polarizability of the $6s7d\ ^3D_1\ |M| = 1$ sub-levels might have been plausibly explained by the coupling with the close $6s8p\ ^3P_1$ state. However, under the two-level approximation, we obtain $\Delta E|_{\text{two-level}} \approx 7\text{ cm}^{-1}$, which is about five times smaller than the actual energy difference of $6s7d\ ^3D_1$ and $6s8p\ ^3P_1$ states [10]. This shows that the two-level approximation breaks down and the mixing with other states is not negligible.

The large polarizability of $6s7d\ ^3D_1\ M = 0$ sublevel cannot be explained by the known odd-parity energy levels. Using the two-level approximation, one odd-parity state with $J = 0$ or $J = 2$ is predicted to be at $\approx 35,673\text{ cm}^{-1}$. However, it is shown in Fig. 1 that $6s8p\ ^3P_1$ is the only odd-parity state known with that energy. As will be discussed in the next subsection, no unidentified “new” state is expected there either. This shows that two-level approximation is not applicable. Nevertheless, there should be at least one $J = 0$ or $J = 2$ odd-parity state lying somewhat below $35,709\text{ cm}^{-1}$, the energy of $6s7d\ ^3D_1$ state, in order to explain the large negative polarizability of this sublevel. This prediction is confirmed in the next subsection.

c. The $5d6d\ ^3D_1$ state. With the electric field applied, the resonance peak of the $5d6d\ ^3D_1$ state is split into two peaks, corresponding to $|M| = 1$ and $M = 0$ sublevels (Fig. 8). The amplitude of the resonance peak of $M = 0$ sublevel is, as expected, much smaller than that of the $|M| = 1$ sublevels. For both curves in Fig. 8, quadratic functions are used in the fitting to determine polarizabilities. The polarizabilities of this state are at least one order of magnitude smaller than others and agree with our estimate based on the known energy levels of barium.

d. The $6s7d\ ^3D_2$ state. The plot of the Stark-induced energy shift of the $6s7d\ ^3D_2$ state as a function of the applied electric field is shown in Fig. 9. For the $M = 0$ sublevel,

a quadratic function is not adequate to fit the data points and the fourth order term is included in the fitting function. With Eq. (15), we determined the polarizability $\alpha(M = 0) = -66.6(5)$ MHz/(kV/cm)² and hyperpolarizability $\gamma(M = 0) = 8(2)$ kHz/(kV/cm)⁴.

The 6s7d ³D₂ $M = 0$ sublevel can be expected to dominantly couple to the 6s8p ³P₁ $M = 0$. The coupling to 6s8p ¹P₁ is suppressed because of the difference in total spins¹. Under the two-level approximation, the derived $\Delta E|_{\text{two-level}} = 103(20)$ cm⁻¹ is consistent with the energy difference between those two states, 93.2(2) cm⁻¹. The derived reduced electric dipole moment $|(6s7d \text{ } ^3D_2 \| D \| 6s8p \text{ } ^3P_1)_{\text{two-level}}| = 22(2)$ ea₀ is not too different from 34.7 ea₀, that we estimate using the Bates-Damgaard approximation using expressions given in [8].

For the $|M| = 1$ and $|M| = 2$ sublevels (as most clearly seen in Fig. 9, for $|M| = 2$) the Stark-induced energy shifts do not obey the electric-field dependence of Eq. (14) and the perturbation theory is not applicable. The enormous shifts of all sublevels require an odd-parity state with $J = 2$ or 3, with energy slightly lower than 35,762.211 cm⁻¹, the energy of 6s7d ³D₂ state. However, it seems that the $M = 0$ sublevel is not coupled to this new state; otherwise the two-level approximation would not apply for $M = 0$ sublevel. Therefore, we expect this new state with $J = 2$. Another constraint on the term of this new state is that the electric dipole moment between this $J = 2$ state and the 6s7d ³D₁ state should be small compared with $(6s7d \text{ } ^3D_1 \| D \| 6s8p \text{ } ^3P_{0,1})$; otherwise it would strongly cancel the contribution of the polarizabilities of the 6s7d ³D₁ state from the 6s8p ³P_{0,1} states. It is known that the electric dipole moment between two states with $\Delta J = -\Delta L$, where L is the orbital angular momentum, is suppressed [8] (See also Table V). Therefore, on the basis of all these arguments, this new state is predicted to be a ³P₂ state. This prediction is confirmed by the observation of one of the Stark-induced transitions discussed in the next subsection. The missing state is most likely 6s8p ³P₂.

The Stark effect of the $|M| = 2$ sublevels could be modelled with a three-level system, consisting of 6s7d ³D₃, 6s7d ³D₂, and 6s8p ³P₂. Notice that although $|6s7d \text{ } ^3D_2 \text{ } |M| = 2\rangle$ sublevels only dominantly couple to $|6s8p \text{ } ^3P_2 \text{ } |M| = 2\rangle$, the two-level approximation is not adequate in this case, because $|6s8p \text{ } ^3P_2 \text{ } |M| = 2\rangle$ is also strongly coupled to $|6s7d \text{ } ^3D_3 \text{ } |M| = 2\rangle$. The couplings to the close-lying states other than these three are suppressed because of the

¹ The spin-orbit interaction can mix the 6s8p ³P₁ and 6s8p ¹P₁ states so that the electric dipole coupling between the 6s7d ³D₂ and 6s8p ¹P₁ states is not zero. This mixing, which is estimated in section V, is negligible in present crude estimation.

difference in total spins or the different configuration of both electrons. With the three-level approximation, we have determined the energy of $6s8p\ ^3P_2$ state as $35,756(1)\text{ cm}^{-1}$ and obtained two reduced electric dipole moments, $|(6s7d\ ^3D_2\|D\|6s8p\ ^3P_2)_{\text{three-level}}| = 16.2(5)\text{ ea}_0$ and $|(6s7d\ ^3D_3\|D\|6s8p\ ^3P_2)_{\text{three-level}}| = 40(2)\text{ ea}_0$. The polarizability of the $|M| = 2$ sublevels is found to be $\alpha(|M| = 2) = -881(13)\text{ MHz}/(\text{kV}/\text{cm})^2$. Knowing $\alpha(|M| = 2)$ and $\alpha(M = 0)$, in the three-level approximation, we obtain $\alpha_0 = -335(13)\text{ MHz}/(\text{kV}/\text{cm})^2$ and $\alpha_2 = -268(13)\text{ MHz}/(\text{kV}/\text{cm})^2$.

B. Observation of the Stark-induced transitions

In this subsection, we discuss the observation of the Stark-induced transitions to the odd-parity states. Within the energy range studied, five Stark-induced transitions are detected and classified into three sets. Each set of resonances is discussed in detail in the following.

Two of the Stark-induced resonances are classified as the first set. According to the electric-field dependence of the amplitudes of the signals, the perturbation theory applies in both cases. The resonance position as a function of the applied electric field is shown in Fig. 10. The fitting function for $|M| = 1$ sublevels is a quadratic function plus a constant term, which corresponds to the energy of the zero-electric-field resonance, which cannot be measured directly in our experiment. For the $M = 0$ sublevel, the fourth order term is necessary and Eq. (14) plus a constant is employed as the fitting function. The derived energies of the zero-electric-field resonance from each curve are $35,668.7(2)$ and $35,668.8(2)\text{ cm}^{-1}$, respectively. The coincidence of the two values shows that they are the split Zeeman sublevels of the same state. The fact that this derived energy coincides with the energy of the $6s8p\ ^3P_1$ state, $35,669.0(2)\text{ cm}^{-1}$ [10], indicates that these two resonance peaks are the Stark-induced transitions to the $|M| = 1$ and $M = 0$ sublevels of this state. The $|M|$ of each curve is determined from the amplitude dependence on laser polarization. From the electric-field dependence of the resonance position, we have determined the polarizabilities of the $6s8p\ ^3P_1$ state (Table II) and the hyperpolarizability $\gamma(M = 0) = -47(11)\text{ kHz}/(\text{kV}/\text{cm})^4$.

One of the Stark-induced resonances is classified as belonging to a set by itself. According to the electric-field dependence of the amplitude of the signal, the perturbation theory applies in this case. The resonance position as a function of the applied electric field is shown in Fig. 11. The data points are fit with Eq. (14) plus a constant term. The polar-

izability can be derived and the position of the zero-electric-field resonance is determined at $35,648.5(1) \text{ cm}^{-1}$. As shown in Fig. 1, no state has been previously identified with this energy. The variation of the amplitude of the signal as a function of the polarizations of the laser beams is consistent with that of a $M = 0$ sublevel. This “new” odd-parity state is probably the missing $6s8p \ ^3P_0$ state. The existence of this state explains the large polarizabilities of the $6s7d \ ^3D_1$ state.

The other two of the Stark-induced resonances are classified as the third set. We have identified them (using the laser-polarization dependence of the signal amplitude) as due to the $|M| = 1$ and $|M| = 2$ sublevels, respectively. From the electric-field dependence of the amplitudes of the signals, the perturbation theory is not applicable in either case. This is consistent with that the Stark-induced energy shifts are almost linearly dependent on the applied electric field (Fig. 12). The data show that the zero-field-energy of a $J \geq 2$ odd-parity state should be within $35,756 \text{ cm}^{-1}$, derived from polynomial fit, and $35,761 \text{ cm}^{-1}$, derived from linear fit. This is consistent with the predicted energy of the $6s8p \ ^3P_2$ state ($35,756(1) \text{ cm}^{-1}$) from the Stark-effect of the $6s7d \ ^3D_2 \ |M| = 2$ sublevels with the three-level approximation. Therefore, these two Stark-induced resonances are probably due to the $|M| = 1$ and $|M| = 2$ sublevels of the $6s8p \ ^3P_2$ state. With a ten-level model, which includes all the states with the energies between $35,600$ and $36,000 \text{ cm}^{-1}$, the energy of the $6s8p \ ^3P_2$ state is determined at $35,757(1) \text{ cm}^{-1}$. The $M = 0$ sublevel is missing because, unlike the $|M| = 1$ and $|M| = 2$ sublevels, it cannot couple to the most closely lying state, $6s7d \ ^3D_2$. Therefore, the Stark-induced transition is weaker. While the fluorescence resulting from the Stark-induced transitions to the $|M| = 1$ and $|M| = 2$ sublevels is already feeble, it is too weak to be detected. The polarizabilities of the $6s8p \ ^3P_2$ state is difficult to determine because of the lack of the low-field data. However, the lower bounds of the scalar and tensor polarizabilities can be determined (Table II).

V. DATA ANALYSIS

In subsection A, we estimate the mixing of states according to the known energy spectrum, including the newly found states. In subsection B, we derive the electric dipole moments from the measured polarizabilities in Table II.

A. Configuration and spin-orbit mixing

There are two multiplets, $6s7d\ ^3D_J$ and $6s8p\ ^3P_J$, in the energy interval under discussion. Both present some irregularities in the fine-structure splittings. We can use them to estimate the mixing with the nearby levels.

The ratio of the “unperturbed” intervals for the $6s7d\ ^3D_J$ multiplet should be $(E_{J=3} - E_{J=2})/(E_{J=2} - E_{J=1}) = 3/2$, according to the Lande interval rule [8]. The most probable explanation for the deviation from this rule is the repulsion between the $6s7d\ ^3D_2$ and $6p^2\ ^3P_2$. Assuming that $6p^2\ ^3P_2$ is the only perturbing source of this multiplet, we have a simplified Hamiltonian for these two states:

$$\begin{pmatrix} E_0(6p^2\ ^3P_2) & \mathcal{V} \\ \mathcal{V} & E_0(6s7d\ ^3D_2) \end{pmatrix}, \quad (19)$$

where the E_0 ’s are the “unperturbed” energies of $6p^2\ ^3P_2$ and $6s7d\ ^3D_2$ states and $\mathcal{V} = \langle 6s7d\ ^3D_2 | V | 6p^2\ ^3P_2 \rangle$, where V is the potential that causes the configuration and spin-orbit mixing. The eigenstates of the matrix are the mixtures of these two states. If we write them in a column vector, they can be expressed as:

$$\begin{pmatrix} \text{“}6p^2\ ^3P_2\text{”} \\ \text{“}6s7d\ ^3D_2\text{”} \end{pmatrix} = \begin{pmatrix} \cos\phi & \sin\phi \\ -\sin\phi & \cos\phi \end{pmatrix} \begin{pmatrix} 6p^2\ ^3P_2 \\ 6s7d\ ^3D_2 \end{pmatrix}, \quad (20)$$

where $\phi = \arctan\{2\mathcal{V}/[E_0(6s7d\ ^3D_2) - E_0(6p^2\ ^3P_2)]\}/2$ is the mixing angle. The mixing “shifts” the energies of the states by $[\sec(2\phi) - 1] \cdot [E_0(6s7d\ ^3D_2) - E_0(6p^2\ ^3P_2)]/2$ in “repulsive” directions. Assuming that $6s7d\ ^3D_{1,3}$ states are unperturbed, we estimate the shift of the level $6s7d\ ^3D_2$ to be 23 cm^{-1} . That gives the mixing angle $\phi \approx \arctan(0.44)$. This two-level model can plausibly explain the large electric dipole moments between the $6p^2\ ^3P_2$ state and the $6s8p\ ^3P_{1,2}$ states since it predicts:

$$\frac{\langle 6s7d\ ^3D_2 | D | 6s8p\ ^3P_1 \rangle}{\langle 6p^2\ ^3P_2 | D | 6s8p\ ^3P_1 \rangle} = \frac{\langle 6s7d\ ^3D_2 | D | 6s8p\ ^3P_2 \rangle}{\langle 6p^2\ ^3P_2 | D | 6s8p\ ^3P_2 \rangle} = \tan\phi. \quad (21)$$

Similar analysis shows that there is an interaction between $6s8p\ ^3P_1$ and $6s8p\ ^1P_1$ states. In the LS -coupling scheme, assuming the coupling with the rest of the states is negligible,

² The interaction with the $6s7d\ ^1D_2$ state is suppressed because of the relatively large energy difference.

we have a simplified Hamiltonian for the 6s8p $^3P_{0,1,2}$ and 1P_1 states:[11]

$$\begin{array}{c} {}^3P_2 \quad {}^3P_1 \quad {}^1P_1 \quad {}^3P_0 \\ \begin{array}{c} {}^3P_2 \\ {}^3P_1 \\ {}^1P_1 \\ {}^3P_0 \end{array} \left(\begin{array}{cccc} F - G - \zeta & 0 & 0 & 0 \\ 0 & F - G - \zeta & \sqrt{2} \zeta & 0 \\ 0 & \sqrt{2} \zeta & F + G & 0 \\ 0 & 0 & 0 & F - G - 2 \zeta \end{array} \right), \end{array} \quad (22)$$

where F is an additive constant, G causes the splitting of the triplet and the singlet, and ζ is from the spin-orbit interaction that causes the splitting of the 3P_J states and the mixing of the 3P_1 and the 1P_1 states. There are only three parameters to determine four energies of the 6s8p multiplets. The eigenvalues of this Hamiltonian fit the observed energies of the 6s8p multiplets very well, deviated by $< 2 \text{ cm}^{-1}$ compared to the $\sim 100 \text{ cm}^{-1}$ energy difference between these four states. The consistency of the LS -coupling scheme with the observed energies of the 6s8p multiplets indicates that the configuration mixing is small.³ The mixing angle between the 3P_1 and the 1P_1 states is $\chi \approx \arctan(0.27)$.

For both cases, because of the non-negligible mixing angles, the mixing should be taken into account in the analysis in the next subsection.

In the LS -coupling scheme, the ratios between the electric dipole moments of the 6s7d 3D_J and 6s8p 3P_J multiplets are given in Table V [8]. Since LS coupling is not exact, we do not expect these relations to be accurate. However, they can give us the estimates for the contributions of the weak couplings.

B. Electric dipole moments derived from experimental data on polarizabilities

In this subsection, we try to derive electric dipole moments from the measured polarizabilities presented in Table II. In Table VI, the angular coefficients from Eqs.(10,12) are tabulated. It simplifies the analysis if one uses combinations of α_0 and α_2 in order to exclude contributions of particular opposite-parity states. These combinations for $J = 1$ and $J = 2$ are given in Table VII. The dipole moments derived in this subsection are listed in Table VIII.

³ Similar analysis of 6s6p multiplets in Ba (and also in other atoms such as Yb) shows larger deviations from the experimental data, which can be explained by stronger configuration mixing due to larger overlap of the wavefunctions of the 6s, 6p, and 5d electrons.

1. *The $6p^2 \ ^3P_2$ state.*

The three dominant coupling states are $6s8p \ ^3P_{1,2}$, and $6s8p \ ^1P_1$. The $5d7p \ ^3F_2$ state is negligible because energy difference is large and the configuration is different by two electrons with $\Delta L = 2$. Using Table VII, we can exclude the contribution from $J = 1$ states by taking the following combination of the scalar and tensor polarizabilities:

$$\alpha_0 + \alpha_2 = +\frac{4}{15} \frac{|\langle 6p^2 \ ^3P_2 || D || 6s8p \ ^3P_2 \rangle|^2}{140(1) \text{ cm}^{-1}}. \quad (23)$$

This gives the dipole moment $|\langle 6p^2 \ ^3P_2 || D || 6s8p \ ^3P_2 \rangle| = 6.0(2) \text{ ea}_0$. Similarly, the contribution from $J = 2$ states can be excluded in a different combination of the polarizabilities.

$$\alpha_0 - \alpha_2 = \frac{4}{15} \left(\frac{|\langle 6p^2 \ ^3P_2 || D || 6s8p \ ^3P_1 \rangle|^2}{52.0(2) \text{ cm}^{-1}} + \frac{|\langle 6p^2 \ ^3P_2 || D || 6s8p \ ^1P_1 \rangle|^2}{276 \text{ cm}^{-1}} \right). \quad (24)$$

The contribution of the $6s8p \ ^1P_1$ state can be estimated:

$$|\langle 6p^2 \ ^3P_2 || D || 6s8p \ ^1P_1 \rangle|^2 \approx \tan^2 \chi \cdot |\langle 6p^2 \ ^3P_2 || D || 6s8p \ ^3P_1 \rangle|^2, \quad (25)$$

This gives the dipole moment $|\langle 6p^2 \ ^3P_2 || D || 6s8p \ ^3P_1 \rangle| = 14.34(6) \text{ ea}_0$. The estimate, Eq.(25), leads to a 0.7% decrease of the dipole moment. Therefore, it is unlikely that this approximation leads to a large error.

2. *The $6s7d \ ^3D_1$ state.*

The four dominant coupling states are the $6s8p \ ^3P_{0,1,2}$, and $6s8p \ ^1P_1$ states. The coupling to the $5d7p \ ^3F_2$ state is negligible because the configurations is different by two electrons and the energy difference is large. The coupling to the $6s8p \ ^3P_2$ state is suppressed because $\Delta J = -\Delta L$, which is strongly suppressed (Table V). By taking the following combination:

$$2\alpha_2 - \alpha_0 = +\frac{2}{3} \frac{|\langle 6s7d \ ^3D_1 || D || 6s8p \ ^3P_0 \rangle|^2}{60.8(1) \text{ cm}^{-1}} - \frac{4}{15} \frac{|\langle 6s7d \ ^3D_1 || D || 6s8p \ ^3P_2 \rangle|^2}{48(1) \text{ cm}^{-1}} \quad (26)$$

$$\approx (1 - 0.025) \frac{|\langle 6s7d \ ^3D_1 || D || 6s8p \ ^3P_0 \rangle|^2}{91.2(2) \text{ cm}^{-1}}, \quad (27)$$

we can derive $|\langle 6s7d \ ^3D_1 || D || 6s8p \ ^3P_0 \rangle| = 15.9(1) \text{ ea}_0$. The estimated contribution of the $6s8p \ ^3P_2$ state changes the dipole moment by $\sim 1\%$, which justifies the estimate.

Another combination of the polarizabilities gives the second equation for this state:

$$\alpha_0 + \alpha_2 = -\frac{1}{3} \frac{|\langle 6s7d \ ^3D_1 || D || 6s8p \ ^3P_1 \rangle|^2}{40.3(2) \text{ cm}^{-1}} + \frac{1}{5} \frac{|\langle 6s7d \ ^3D_1 || D || 6s8p \ ^3P_2 \rangle|^2}{48(1) \text{ cm}^{-1}} \quad (28)$$

$$+ \frac{1}{3} \frac{|\langle 6s7d \ ^3D_1 || D || 6s8p \ ^1P_1 \rangle|^2}{183 \text{ cm}^{-1}} \quad (29)$$

Again, we estimate $|\langle 6s7d \ ^3D_1 || D || 6s8p \ ^3P_2 \rangle|$ with Table V and $|\langle 6s7d \ ^3D_1 || D || 6s8p \ ^1P_1 \rangle|^2 \approx \tan^2 \chi \cdot |\langle 6s7d \ ^3D_1 || D || 6s8p \ ^3P_1 \rangle|^2$. This derives the dipole moment $|\langle 6s7d \ ^3D_1 || D || 6s8p \ ^3P_1 \rangle| = 12.4(2) \text{ ea}_0$. Note that the ratio of the dipole moments $|\langle 6s7d \ ^3D_1 || D || 6s8p \ ^3P_0 \rangle|$ and $|\langle 6s7d \ ^3D_1 || D || 6s8p \ ^3P_1 \rangle|$ is 1.28(1), which differs only by 10% from the *LS*-coupling prediction (Table V).

3. The 6s7d 3D_2 state.

The possible dominant coupling states are 6s8p $^3P_{1,2}$, 1P_1 and 5d7p 3F_2 states. Again, we can take the different combinations of the scalar and tensor polarizabilities to extract the contribution of $J = 1$ or $J = 2$ states.

$$\alpha_0 + \alpha_2 = -\frac{4}{15} \left(\frac{|\langle 6s7d \ ^3D_2 || D || 6s8p \ ^3P_2 \rangle|^2}{5(1) \text{ cm}^{-1}} + \frac{|\langle 6s7d \ ^3D_2 || D || 5d7p \ ^3F_2 \rangle|^2}{-473 \text{ cm}^{-1}} \right), \quad (30)$$

We can neglect the second term in the right hand side of Eq.(30) considering the relatively large uncertainty in the denominator of the first term. It follows that $|\langle 6s7d \ ^3D_2 || D || 6s8p \ ^3P_2 \rangle| = 14(2) \text{ ea}_0$. Note that Table V predicts $|\langle 6s7d \ ^3D_2 || D || 6s8p \ ^3P_2 \rangle| = |\langle 6s7d \ ^3D_1 || D || 6s8p \ ^3P_1 \rangle|$, so we have reasonable agreement with the *LS*-coupling. The second equation is:

$$\alpha_2 - \alpha_0 = \frac{4}{15} \left(\frac{|\langle 6s7d \ ^3D_2 || D || 6s8p \ ^3P_1 \rangle|^2}{93.2(2) \text{ cm}^{-1}} + \frac{|\langle 6s7d \ ^3D_2 || D || 6s8p \ ^1P_1 \rangle|^2}{-130 \text{ cm}^{-1}} \right) \quad (31)$$

$$\approx (1 - 0.052) \frac{|\langle 6s7d \ ^3D_2 || D || 6s8p \ ^3P_1 \rangle|^2}{348.8 \text{ cm}^{-1}}. \quad (32)$$

This gives the dipole moment $|\langle 6s7d \ ^3D_2 || D || 6s8p \ ^3P_1 \rangle| = 21(3) \text{ ea}_0$. The ratio between $|\langle 6s7d \ ^3D_2 || D || 6s8p \ ^3P_1 \rangle|$ and $|\langle 6s7d \ ^3D_2 || D || 6s8p \ ^3P_2 \rangle|$ is 1.5(4), which is consistent with the prediction of Table V. The ratio between $|\langle 6p^2 \ ^3P_2 || D || 6s8p \ ^3P_1 \rangle|$ and $|\langle 6s7d \ ^3D_2 || D || 6s8p \ ^3P_1 \rangle|$ is 0.7(1), which is somewhat larger than the prediction of Eq. (21), $\tan \phi \approx 0.44$.

4. The 5d6d 3D_1 state.

For this state, we can expect that the largest contribution of the polarizabilities is from the coupling to the 5d7p 3F_2 state, which is counterbalanced by four smaller couplings to the closer levels. This may explain the smallness of both polarizabilities of this level. However, the quantitative analysis is hampered by the large number of contributions. Thus, we are not able to use experimental data for this state in our analysis.

5. The 6s8p 3P_0 state.

The dominant coupling states are the 6s7d 3D_1 and 5d6d 3D_1 states. We can use Eq.(27) to calculate the contribution of the 6s7d 3D_1 state and estimate the coupling to the 5d6d 3D_1 state.

$$\alpha_0 = \left(-\frac{2}{3}\right) \left(\frac{|\langle 6s7d \ ^3D_1 || D || 6s8p \ ^3P_0 \rangle|^2}{-60.8(1) \text{ cm}^{-1}} + \frac{|\langle 5d6d \ ^3D_1 || D || 6s8p \ ^3P_0 \rangle|^2}{-285.3(1) \text{ cm}^{-1}} \right) \quad (33)$$

$$\approx \frac{1}{0.975} (2\alpha_2 - \alpha_0)_{6s7d \ ^3D_1} + \frac{2}{3} \frac{|\langle 5d6d \ ^3D_1 || D || 6s8p \ ^3P_0 \rangle|^2}{285.3(1) \text{ cm}^{-1}} \quad (34)$$

This gives the dipole moment $|\langle 5d6d \ ^3D_1 || D || 6s8p \ ^3P_0 \rangle| = 14(2) \text{ ea}_0$, which is unexpectedly large considering the configurations of these two states are different by two electrons. This large dipole moment probably means that the 5d6d 3D_1 state interacts with the 6s7d 3D_1 state. This interaction can influence the mixing angle ϕ , which is derived under the assumption that the 6s7d $^3D_{0,2}$ states are unperturbed by the configuration or spin-orbit mixing. This interaction “shifts” the 6s7d 3D_2 state downwards and makes mixing angle ϕ larger, which is consistent with our expectation of larger $\tan(\phi)$ to explain the large $|\langle 6p^2 \ ^3P_2 || D || 6s8p \ ^3P_1 \rangle|$ dipole moment.

6. The 6s8p 3P_1 state.

The dominant coupling states for the 6s8p 3P_1 state are $6p^2 \ ^3P_2$, 6s7d 3D_1 , and 5d6d 3D_1 states. We have derived all major contributions to the polarizabilities of the 6s8p 3P_1 state. Therefore, we can use the polarizabilities to check our model for consistency. The scalar

polarizability is given by the following expression:

$$\alpha_0 = -\frac{2}{9} \left(\frac{|\langle 6p^2 \ ^3P_2 || D || 6s8p \ ^3P_1 \rangle|^2}{52.0(2) \text{ cm}^{-1}} + \frac{|\langle 6s7d \ ^3D_1 || D || 6s8p \ ^3P_1 \rangle|^2}{-40.3(2) \text{ cm}^{-1}} \right. \\ \left. + \frac{|\langle 6s7d \ ^3D_2 || D || 6s8p \ ^3P_1 \rangle|^2}{-93.2(2) \text{ cm}^{-1}} + \frac{|\langle 5d6d \ ^3D_1 || D || 6s8p \ ^3P_1 \rangle|^2}{-265 \text{ cm}^{-1}} \right). \quad (35)$$

Using the experimental data in Table II and Eqs.(24,28,32), we have:

$$\frac{|\langle 5d6d \ ^3D_1 || D || 6s8p \ ^3P_1 \rangle|^2}{1193 \text{ cm}^{-1}} = 0.8(5) \text{ ea}_0^2/\text{cm}^{-1}. \quad (36)$$

This is almost consistent with zero contribution from the $5d6d \ ^3D_1$ state. However, because of the large error in Eq.(36), we cannot obtain significant bound on the dipole moment $|\langle 5d6d \ ^3D_1 || D || 6s8p \ ^3P_1 \rangle|$. The tensor polarizability can be expressed as:

$$\alpha_2 = \frac{1}{45} \frac{|\langle 6p^2 \ ^3P_2 || D || 6s8p \ ^3P_1 \rangle|^2}{52 \text{ cm}^{-1}} - \frac{1}{9} \frac{|\langle 6s7d \ ^3D_1 || D || 6s8p \ ^3P_1 \rangle|^2}{-40 \text{ cm}^{-1}} \\ + \frac{1}{45} \frac{|\langle 6s7d \ ^3D_2 || D || 6s8p \ ^3P_1 \rangle|^2}{-93 \text{ cm}^{-1}} - \frac{1}{9} \frac{|\langle 5d6d \ ^3D_1 || D || 6s8p \ ^3P_1 \rangle|^2}{-265 \text{ cm}^{-1}}. \quad (37)$$

With similar method, we get:

$$\frac{|\langle 5d6d \ ^3D_1 || D || 6s8p \ ^3P_1 \rangle|^2}{2385 \text{ cm}^{-1}} \approx 0.0(1) \text{ ea}_0^2/\text{cm}^{-1}. \quad (38)$$

This is consistent with the zero contribution from the $5d6d \ ^3D_1$ state and gives an upper bound:

$$|\langle 5d6d \ ^3D_1 || D || 6s8p \ ^3P_1 \rangle| \leq 15 \text{ ea}_0. \quad (39)$$

VI. SYSTEMATIC UNCERTAINTIES

The systematic uncertainties in this work come in two ways. One is from the simplified models used in the data analysis. The other is from the limited sensitivities of the apparatus. It is found that the systematic uncertainties are mostly from the simplified models. To take them into account, we multiply the statistical uncertainties by the square-root of the reduced χ^2 to be the presented uncertainties.

The possible sources of the systematic uncertainties from the limited sensitivity of the apparatus are discussed. It is found that the dominant errors come from the drift of the frequency markers (in the first part of the experiment) and the uncertainty in the reading of the grating position (in the second part of the experiment).

In the first part of the experiment, a temporal drift of the frequency-markers was observed. The overall drift is about 10 GHz over ~ 4 hours of run time. The effect is consistent with what we expect from the thermal variation of the index of refraction and the thermal expansion of the glass heated by the laser and/or variations of room temperature. To account for the drift, we recorded zero-electric-field scans before and after each non-zero-field scan. The drifts of the frequency markers relative to the positions of the zero-electric-field resonance peaks were thus observed and recorded. Because the drift is a smooth function of time, knowing at what time a given scan is recorded, we can determine the reference point of the energy shifts when the electric field is applied from the positions of the two adjacent zero-electric-field resonance peaks. This systematic error can be reduced to ≈ 500 MHz. However, this is still the dominant source of the systematic uncertainties.

In the second part of the experiment, it is more difficult to determine the Stark-induced energy shift because the signal is only present when the electric field is applied. In order to reduce the error from the temporal drift of the reading of the grating position, we use the same method, but instead of recording the position of a resonance at zero electric field, we record that of transition to $6p^2\ ^3P_2$, whose energy is well-determined, before and after each measurement of the resonance of the Stark-induced transition. This method reduces the systematic error to ≈ 6 GHz. This is the dominant source of the systematic uncertainties.

The electric field calibration was discussed in Ref.[7]. The high voltage output is calibrated to 0.015%. The electrode spacing is calibrated to 0.02%. This determines the electric field with 0.03% precision. Therefore, the systematic uncertainty of the electric field is negligible.

In the presence of strong laser pulses, the energy of a state is shifted, due to the dynamic Stark effect. To avoid this effect, we temporally separate the two pulses by 20 – 30 ns and attenuate the powers of lasers, so they barely saturate the transitions. We have verified that the measured polarizabilities are independent of the temporal separation of the two laser pulses or the laser powers, so the dynamic Stark effect is negligible in our experiments.

The errors from the electronic noises, the uncertainties of the readouts of the barometer and CAMAC modules, and the hyperfine structures of the barium isotopes with non-zero nuclear spin (^{135}Ba and ^{137}Ba , both with $I = 3/2$) are also estimated. It is found that these systematic errors are negligible.

VII. CONCLUSIONS

In this work, we have measured the scalar and tensor polarizabilities of four even-parity states of barium ranging from 35,600 to 36,000 cm^{-1} , and the hyperpolarizabilities of two of those four states. Three of these states have unusually large polarizabilities which exceed the value that might be expected from the known energy levels of barium by more than two orders of magnitude. Our experimental data suggest the existence of two “new” states. These two states have been identified by direct laser spectroscopy of the Stark-induced transitions and their energies have been determined to within $\approx 1 \text{ cm}^{-1}$. The polarizabilities of two odd-parity states excited via the Stark-induced transitions are measured. Using the polarizabilities measured in this work, we have also derived seven electric dipole moments. Their relative values are consistent with the prediction of the LS -coupling scheme.

Acknowledgments

The authors wish to thank V. V. Yashchuk and D. English for help with the experiments and useful discussions, and D. P. DeMille, B. P. Das, W. Gawlik, W. C. Martin and M. Kuchiev for helpful advice. This research was supported by the National Science Foundation Career grant PHY-9733479 and the Miller Institute for Basic Research in Science.

-
- [1] R. H. Rinkleff and R. Wehmschulte, *Z. Phys. D* **39**, 139 (1997).
 - [2] J. Li and W. A. Van Wijngaarden, in *QELS '95. Summaries of Papers Presented at the Quantum Electronics and Laser Science Conference* (1995), vol. 16 of *Technical Digest Series Conference Edition*, p. 193.
 - [3] P. Kulina and R. H. Rinkleff, *Z. Phys. A* **318**, 251 (1984).
 - [4] P. Kulina and R. H. Rinkleff, *Z. Phys. A* **313**, 241 (1983).
 - [5] K. A. H. van Leeuwen, W. Hogervorst, and B. H. Post, *Phys. Rev. A* **28**, 1901 (1983).
 - [6] D. English, D. Budker, and D. DeMille, in *proceedings of the International Conference on Spin-Statistics Connection and Commutation Relations: Experimental Tests and Theoretical*

Implications, edited by R. C. Hilborn and G. M. Tino (Anacapri, Italy, 2000), vol. 545 of *AIP Conf. Procs.*, p. 281.

- [7] S. M. Rochester, C. J. Bowers, D. Budker, D. DeMille, and M. Zolotarev, *Phys. Rev. A* **59**, 3480 (1999).
- [8] I. I. Sobel'man, *Atomic spectra and radiative transitions* (Springer-Verlag, Berlin, 1992).
- [9] M. G. Kozlov and S. G. Porsev, *Eur. Phys. J. D* **5**, 59 (1999).
- [10] J. A. Armstrong, J. J. Wynne, and P. Esherick, *J. Opt. Soc. Am.* **69**, 211 (1979).
- [11] E. U. Condon and G. H. Shortley, *The theory of atomic spectra* (Cambridge university press, Cambridge, 1963).

Figures

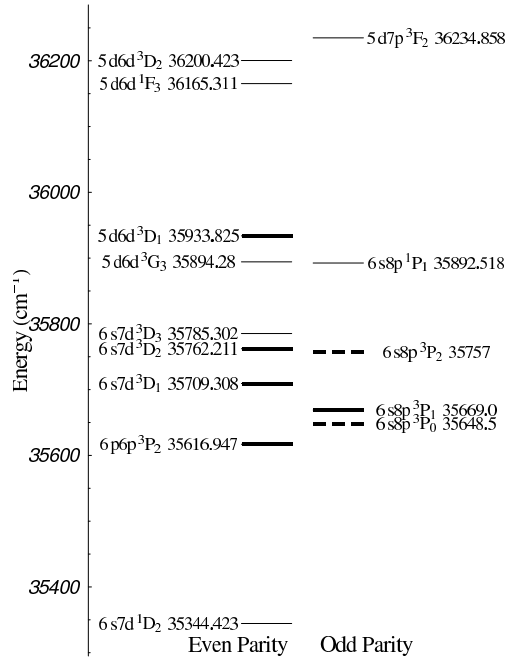


FIG. 1: The energy-level diagram of barium ranging from 35,300 to 36,300 cm^{-1} . The dashed lines are the suggested “new” energy levels. The seven bold lines are the states whose polarizabilities are measured in this work.

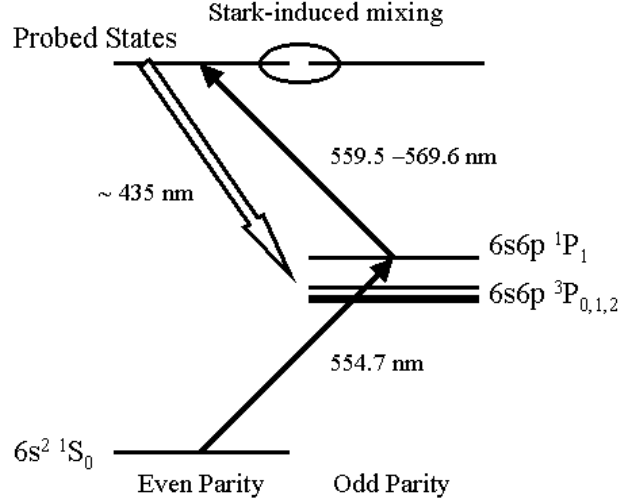


FIG. 2: The excitation-detection scheme. Solid arrows indicate laser excitation; the hollow arrow indicates fluorescence. The odd-parity states can be excited due to the Stark-induced mixing.

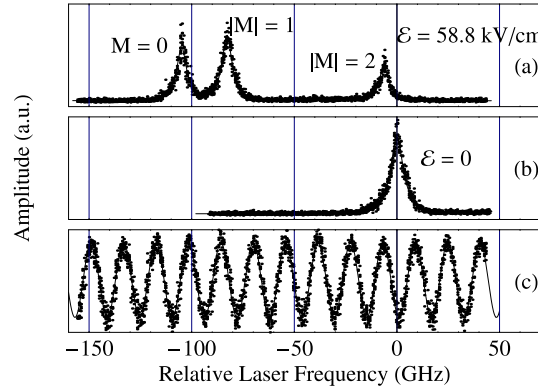


FIG. 3: The scan patterns for the $6p^2 \ ^3P_2$ state: (a) amplitude of fluorescence with an electric field applied; (b) amplitude of fluorescence with no electric field; (c) amplitude of the reflection from the etalon used as a frequency marker. The data points in (a) and (b) are fit by Lorentzian functions. The data points in (c) are fit by a sinusoidal function.

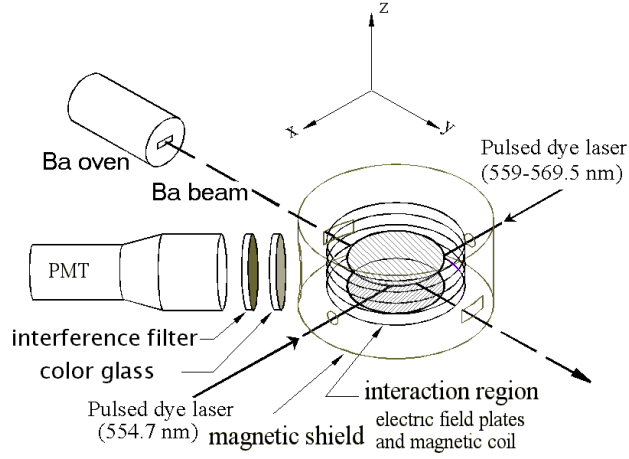


FIG. 4: Block diagram of the apparatus.

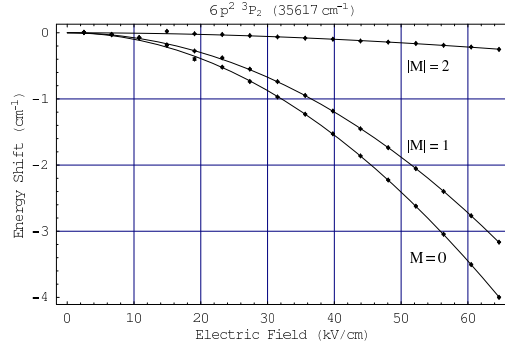


FIG. 5: The Stark splitting and shift for the resonance of the $6p^2 \ ^3P_2$ state. The data points are fit by Eq.(14).

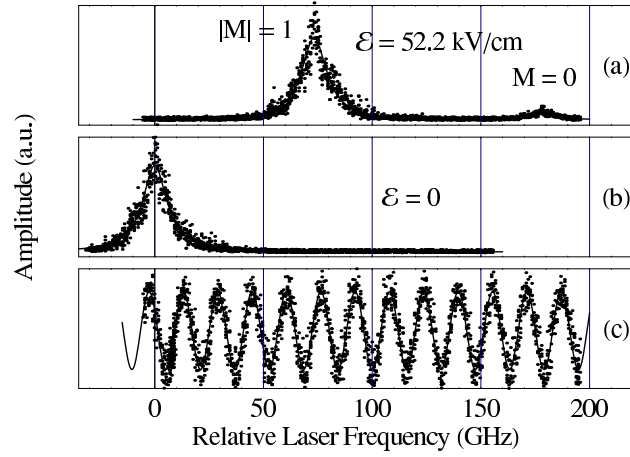


FIG. 6: The scan patterns for the $6s7d\ ^3D_1$ state: (a) amplitude of fluorescence with an electric field applied; (b) amplitude of fluorescence with no electric field; (c) amplitude of the reflection from the etalon used as a frequency marker. The data points in (a) and (b) are fit by Lorentzian functions. The data points in (c) are fit by a sinusoidal function.

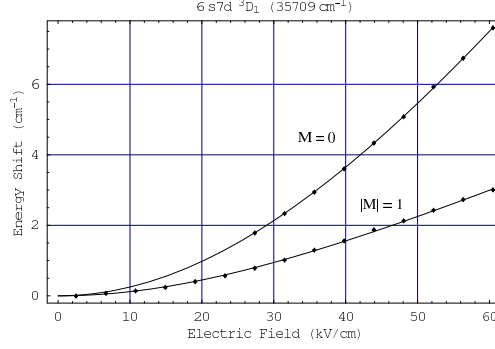


FIG. 7: The Stark splitting and shift for the resonance of the $6s7d\ ^3D_1$ state. The data points are fit by Eq.(14).

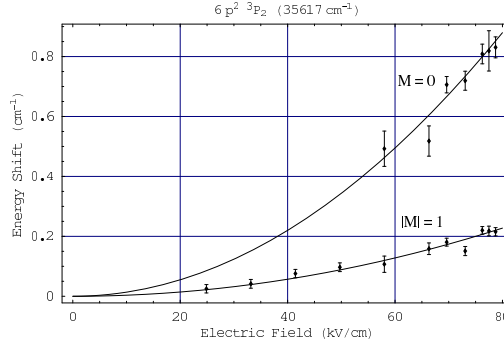


FIG. 8: The Stark splitting and shift for the resonance of the $5d6d\ ^3D_1$ state. The data points are fit by quadratic functions.

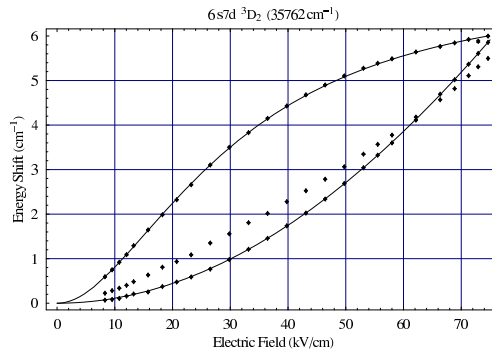


FIG. 9: The Stark splitting and shift for the resonance of the $6s7d\ ^3D_2$ state. The data points corresponding to $M = 0$ sublevel are fit by the exact solutions of the two-level Hamiltonian. The data points corresponding to $|M| = 2$ sub-levels are fit by the exact solutions of the three-level Hamiltonian. The data points corresponding to $|M| = 1$ sub-levels cannot be fit by quadratic functions or modelled by a two- or three-level system.

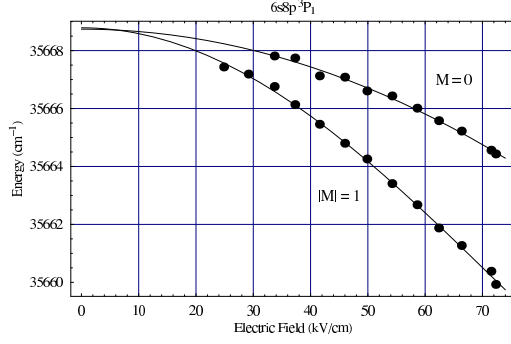


FIG. 10: The Stark splitting and shift for the resonance of the $6s8p\ ^3P_1$ state. The data points corresponding to $|M| = 1$ sub-levels are fit by a quadratic function. The data points corresponding to $M = 0$ sub-level are fit by Eq.(14).

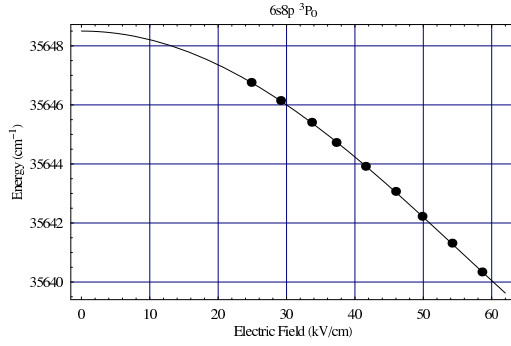


FIG. 11: The Stark shift for the resonance of the $6s8p\ ^3P_0$ state. The data points are fit by Eq.(14).

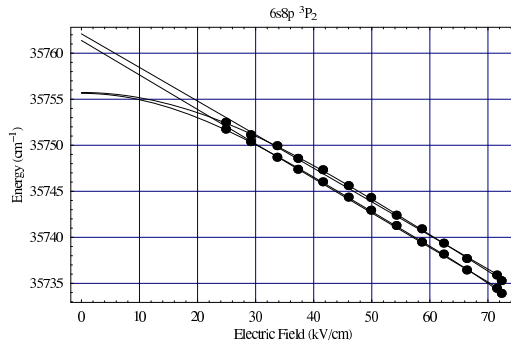


FIG. 12: The Stark splitting and shift for the resonance of the $6s8p\ ^3P_2$ state. The data points corresponding to $|M| = 1$ and $|M| = 2$ sublevels are fit by both a linear function and a sixth-order polynomial functions. The linear fit gives an upper bound of the energy of $6s8p\ ^3P_2$ state while the sixth-order polynomial fit gives a lower bound.

Tables

TABLE I: The relation between the polarizations of laser beams and the excited Zeeman sublevels of a state with total angular momentum J , which are excited by two E1 transitions from the $J = 0$ ground state via a $J = 1$ intermediate state.

J	Polarizations of laser beams		
	z, z	y, z or z, y	y, y
0	$M = 0$	-	$M = 0$
1	-	$ M = 1$	-
2	$M = 0$	$ M = 1$	$ M = 0, 2$

TABLE II: Observed scalar and tensor polarizabilities, in units of $\text{MHz}/(\text{kV}/\text{cm})^2$

State	α_0	α_2
$6p^2\ ^3P_2$	31.05(9)	-27.3(1)
$6s7d\ ^3D_1$	-93(1)	26.6(5)
$6s7d\ ^3D_2$	-335(13)	-268(13)
$5d6d\ ^3D_1$	-4.2(2)	2.0(1)
$6s8p\ ^3P_0$	176(3)	-
$6s8p\ ^3P_1$	97(6)	24(3)
$6s8p\ ^3P_2$	≥ 370	≥ 60

TABLE III: Observed scalar and tensor hyperpolarizabilities in units of $\text{kHz}/(\text{kV}/\text{cm})^4$

State	γ_0	γ_2	γ_4
$6p^2 \ ^3P_2$	$-2.2(16)$	$0(1)$	$-0.6(3)$
$6s7d \ ^3D_1$	$61(3)$	$-5(2)$	—

TABLE IV: Estimated reduced electric dipole moments in units of ea_0 with the two- or three-level approximation.

Reduced dipole moment	Experiment	Bates-Damgaard
$ (6p^2 \ ^3P_2 \ D \ 6s8p \ ^3P_1) _{\text{two-level}}^a$	$14.5(3)$	N/A
$ (6s7d \ ^3D_2 \ D \ 6s8p \ ^3P_1) _{\text{two-level}}$	$22(2)$	34.7
$ (6s7d \ ^3D_2 \ D \ 6s8p \ ^3P_2) _{\text{three-level}}^a$	$16.2(5)$	15.5
$ (6s7d \ ^3D_3 \ D \ 6s8p \ ^3P_2) _{\text{three-level}}^a$	$40(2)$	44

^aThe levels are designated by their nominal or proposed configurations (see text).

TABLE V: Relative values of the reduced matrix elements between the levels of the $6s7d \ ^3D_J$ and $6s8p \ ^3P_J$ multiples in pure LS -coupling.

	$6s8p \ ^3P_0$	$6s8p \ ^3P_1$	$6s8p \ ^3P_2$
$6s7d \ ^3D_1$	$\sqrt{20}$	$\sqrt{15}$	1
$6s7d \ ^3D_2$	0	$\sqrt{45}$	$\sqrt{15}$
$6s7d \ ^3D_3$	0	0	$\sqrt{84}$

TABLE VI: Angular coefficients for α_0 and α_2 .

$J_0 : J_1$	0	1	2	3
0	$-2/3 \quad 0$	$-2/3 \quad 0$		
1	$-2/9 \quad +2/9$	$-2/9 \quad -1/9$	$-2/9 \quad +1/45$	
2		$-2/15 \quad +2/15$	$-2/15 \quad -2/15$	$-2/15 \quad +4/105$
3			$-2/21 \quad +2/21$	$-2/21 \quad -5/42$

TABLE VII: Combinations of α_0 and α_2 that can simplify the analysis.

$J_0 = 1$	$J_0 = 2$	does not depend on
-----------	-----------	--------------------

$\alpha_0 + \alpha_2$		$J_1 = 0,$
$\alpha_0 - 2\alpha_2$	$\alpha_0 + \alpha_2$	$J_1 = 1,$
$\alpha_0 + 10\alpha_2$	$\alpha_0 - \alpha_2$	$J_1 = 2,$
	$2\alpha_0 + 7\alpha_2$	$J_1 = 3.$

TABLE VIII: Electric dipole moments (in units of ea_0) derived from the polarizabilities measured in this work.

	6s8p 3P_0	6s8p 3P_1	6s8p 3P_2
6p ² 3P_2	0	14.34(6)	6.0(2)
6s7d 3D_1	15.9(1)	12.4(2)	-
6s7d 3D_2	0	21(3)	14(2)
5d6d 3D_1	14(2)	≤ 15	-